Shape Representation Using a Generalized Potential Field Model

Narendra Ahuja, *Fellow*, *IEEE*, and

Jen-Hui Chuang, *Member*, *IEEE*

Abstract—This paper is concerned with efficient derivation of the medial axis transform of a two-dimensional polygonal region. Instead of using the shortest distance to the region border, a potential field model is used for computational efficiency. The region border is assumed to be charged and the valleys of the resulting potential field are used to estimate the axes for the medial axis transform. The potential valleys are found by following force field, thus, avoiding two-dimensional search. The potential field is computed in closed form using the equations of the border segments. The simple Newtonian potential is shown to be inadequate for this purpose. A higher order potential is defined which decays faster with distance than as inverse of distance. It is shown that as the potential order becomes arbitrarily large, the axes approach those computed using the shortest distance to the border. Algorithms are given for the computation of axes, which can run in linear parallel time for part of the axes having initial guesses. Experimental results are presented for a number of examples.

Index Terms—Generalized potential, Newtonian potential, topology, medial axis, symmetric axis transform, skeletonization, distance transform.

————————————— ◆ —————————————

1   INTRODUCTION

THIS paper is concerned with obtaining shape representations such as the medial axis transform (MAT) and the generalized cylinder representation in a computationally efficient manner. Commonly, such representations are derived first by computing a distance transform which yields the shortest distance from each pixel to region border, or equivalently, by identifying at each pixel the largest possible size of the primitive of a given shape such that it is entirely contained in a region to be represented. The representation is derived by identifying the primitives having locally maximal sizes. Such approaches are straightforward but computationally expensive since the distance computation must be performed at each pixel. The efficiency of the approach presented in this paper results from the use of an intermediate, analog representation of the given shape information as a potential field. The use of potential field representation helps avoid the expensive task of computing the distance transform at each pixel, and the subsequent elaborate search for the primitives of the desired representation. Instead, the computation is limited approximately to the locations of the locally maximal primitives. The computation of the potential field itself, in the approach presented, is performed efficiently if the shape information is given in a compact form, e.g., as a set of equations each specifying one of the segments in a piecewise continuous representation of the surface. Such a compact description may be directly available as a part of the specification of the given object shape, or it may be derived from the given object data such as its surface or volume description.

Although the approach presented applies to three dimensions, for concreteness, we will confine the detailed discussion to

———————————————

• *N. Ahuja is with the Beckman Institute, University of Illinois, 405 N. Mathews Avenue, Urbana, IL 61801. E-mail: ahuja@vision.csl.uiuc.edu.*
• *J.-H. Chuang is with the Department of Computer and Information Science, National Chiao Tung University, Hsinchu, Taiwan 30010, Republic of China. E-mail: jchuang@cis.nctu.edu.tw.*

two-dimensional (2D) images. Section 2 reviews the definitions of MAT, and the algorithms for their computation reported in the literature. Section 3 describes the motivation for our potential field approach and presents an overview of the approach. Section 4 describes a potential field-based algorithm for computing the MAT. Section 5 presents implementation details and experimental results. Section 6 presents a brief comparison with other approaches. Section 7 presents concluding remarks.

2   THE MAT

The medial axis transform of a shape is defined in terms of the medial axis which is the loci of those points which are equidistant from at least two points along the region border [1]. Thus, the medial axis is composed of the centers of "locally maximal" discs, defined as discs that are as large as they can be without crossing the region border but are not contained in any other locally maximal discs. More formally, let B denote the set of boundary points and let the distance function, or distance transform,

$$d(\mathbf{x}, B) = \inf_{\mathbf{y} \in B} d(\mathbf{x}, \mathbf{y}), \tag{1}$$

denote the minimal distance between a point $\mathbf{x}$ in the region to be represented and the set B. Then for any point $\mathbf{x}$ in the region, if $d(\mathbf{x}, B) = d(\mathbf{x}, \mathbf{y}) = d(\mathbf{x}, \mathbf{z})$ for at least two distinct boundary points $\mathbf{y}$ and $\mathbf{z}$, $\mathbf{x}$ is on the medial axis. The medial axis and the radii of the maximal discs associated with each axis point together define the MAT representation. Fig. 1b shows the MAT skeleton for the rectangular region shown in Fig. 1a.
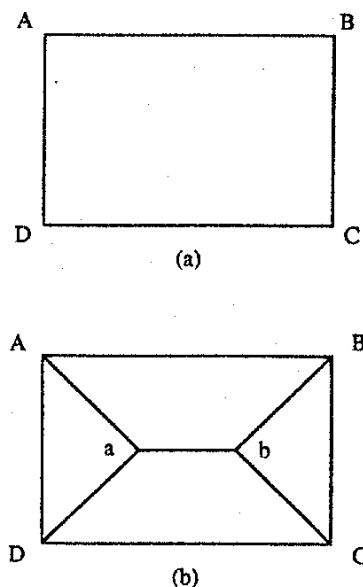

Fig. 1. (a) A rectangle *ABCD*; (b) its medial axis (consisting of segments *Aa*, *Bb*, *Cb*, *Da*, and *ab*).

The points along skeleton curves are local maxima of the shortest distance to the border in the neighborhood of the curves. Thus, the skeleton consists of distance "ridges" which are 1D local maxima of the shortest distance in the direction across the ridges. As an example, for the special case of polygonal regions, these ridge curves are piecewise smooth and consist of linear and parabolic segments. The curves meet at vertices which are local 2D maxima of the shortest distance to the border, i.e., at distance "peaks." The locations and the radii of the discs comprise a representation of the original shape since the represented region is exactly the union of the MAT discs. The use of the disc shape is

motivated by the property that the (Euclidean) distance of the disc center is the same from all points on its border. Since one could use other types of distance, especially for digital images [2], [3], [4], [5], [6], [7], one could use other kinds of "discs," e.g., squares.

A number of algorithms developed to obtain the skeleton of a digital image region explicitly compute the distance transform for each point inside the region. Then, the definition of the locally maximal discs is used in a straightforward way to identify centers of such discs and, thus, the skeleton. The basic definition of MAT is applied in [8] to piecewise uniform gray level images by using squares as shape primitives. Continuous medial axes are obtained in [9] and [10] by following the ridges in the distance transform. A graph representation, called medial line, is used in [11] to join disconnected medial axis segments detected as local maxima of the chessboard distance transform. The ridge points in different distance transforms are detected and connected in [12] to form skeletons. The propagation and extinction of the fire in the grass fire model are directly used to obtain the skeleton in [13]. An algorithm for determining skeletons of polygonal regions based on the same propagation process is presented in [14]. While the computing time is said to be roughly proportional to the number of edges of the polygon, the algorithm is complicated to program. It is shown in [15] that the skeletonization problem is linearly reducible to the construction of generalized Voronoi diagram. O(n log n) algorithms are presented in [15] and [16] for the construction of the skeleton of a simple polygon which has n border segments. [17] presents an algorithm with similar complexity for a set of circular and straight line segments.

3 MOTIVATION AND APPROACH

The computation of the shortest distance to the border is the heart of obtaining the MAT. It requires at each pixel a nonlinear (minimization) operation over shortest distance to *all* border pixels. The axes are given by the locations of the 1D or 2D local maxima of the above shortest distance function. Because of the nonlinear nature of shortest distance computation, the local maxima must be found by explicit spatial search for them. Since, in general, no initial knowledge about the axes is available, the shortest distance function must be computed over the entire region and then the maxima found.

The motivation for the approach presented in this paper is to significantly reduce the computational cost of deriving the medial axis. We achieve this by compressing information about the distances of an interior point to different border points into a single scalar, called potential, which is derived from the distances from the interior point to all border points. Thus, the main feature of our approach is to replace the nonlinear distance transform that computes the local maxima of distance to nearest border point(s), with a linear transform that accumulates distance sensitive contributions from *all* border points. Given the potential field, it is possible to identify the axes without performing the O(*region area*) computation of the shortest distance, by limiting the computation to the vicinity of the desired axes. This is because the forces resulting from the potential field can be used to reach and follow the axes without explicitly performing any area based search for minima.

Analytic expressions for skeleton segments are derived in [15] and [16] with good computational complexity as mentioned earlier. However, the corresponding algorithms are complicated to program and the complete skeleton has to be computed first even if part of it is needed. The proposed approach, on the other hand, obtains samples along the skeleton (potential valleys) by following the negative gradient direction of the potential function. The associated algorithm is extremely simple and the samples can be obtained only for selected portion of the skeleton, making it very efficient. For a given number of skeleton segments

to be obtained, the computation time is proportional to the number of edges of the polygon. The proposed approach can also be generalized to the 3D space with little change in the computational complexity [18]. In the rest of this section, we will present an overview of our approach.

We assume that the boundary of each region carries an electric charge which gives rise to a scalar potential field. The magnitude of the field is infinity at the boundary and decreases with increasing distance from the boundary. The points along potential valleys (or trajectories of 1D potential minima) are related to branches of the MAT skeleton, and the points which are 2D potential minima are related to vertices of the MAT skeleton. To determine the skeleton, we start at an arbitrary point interior to the region, and follow the direction of the force at the point to reach the skeleton. Once we are on the skeleton, we track it by following the directions determined by the force or the local potential variation. Because the force direction depends upon all border points, not just the nearest ones, the result contains only coarse MAT information. Refinements are then made in the definition of the potential to compute an accurate MAT. To do this, the rate of decay of potential with distance from a border point is increased to reduce the influence on potential values (and hence, on the estimate of MAT) of border points which are not the nearest ones. This refinement is the price paid to avoid the more expensive computation of the nonlinear distance transform, thus representing a cost trade-off.

The potential field can be computed by adding contributions from individual pixels along the region border. However, if a (piecewise) analytic description of the border is available, then the potential field may be computed in closed form for entire border (segments), rather than one pixel at a time, and hence, much more efficiently. In the following sections, we will present algorithms that implement the approach outlined above.

4 2D MAT FOR POLYGONAL REGIONS

In this section, we will develop a potential field based algorithm for the computation of MAT for a 2D polygonal region in three stages. We will start with a preliminary algorithm which uses the Newtonian potential and captures the basic notions and motivations for our approach summarized in Section 3. We will then describe some problems with this simplistic algorithm and present a second algorithm that uses a generalized definition of potential to avoid the above problems, giving a satisfactory MAT. This will be followed by a third algorithm which performs the same computation as the second algorithm but does so more efficiently. This algorithm will serve as our final algorithm for MAT computation for polygonal regions.

4.1 A Newtonian Potential Based MAT Algorithm

For the preliminary algorithm (see also [19]), we will assume that the potential due to a border point is Newtonian, i.e., it is inversely proportional to the distance from the border point. When the region border is specified as a polygon, the overall potential field can be computed as a linear superposition of the fields due to individual border segments. We now obtain a closed form expression for the Newtonian potential due to a line segment. Without the loss of generosity, a special configuration is assumed for the line segment to simplify the discussion.

4.1.1 Newtonian Potential Due to a Line Segment

Consider a point A at $(0, y_0 \neq 0)$ and a finite line charge on x-axis with a unit charge density uniformly distributed between $x = x_1$ and $x = x_2$, as shown in Fig. 2. The Newtonian potential at point A due to a point $(x, 0)$ of the line charge is defined as

$$\frac{1}{r} = \frac{1}{\sqrt{x^2 + y_0^2}}, \qquad x_1 \leq x \leq x_2, \tag{2}$$

where r is the distance between these two points. The total potential due to the whole line segment can then be calculated as

$$\phi_A = \int_{x_1}^{x_2} \frac{dx}{\sqrt{x^2 + y_0^2}} = \log\left| x + \sqrt{x^2 + y_0^2} \right| \Big|_{x_1}^{x_2}. \quad (3)$$

Due to the similarity of their definitions, the potential and the distance functions have similar spatial structures, e.g., peaks, valleys, and ridges. In Fig. 3, the potential functions are shown for some polygonal regions.
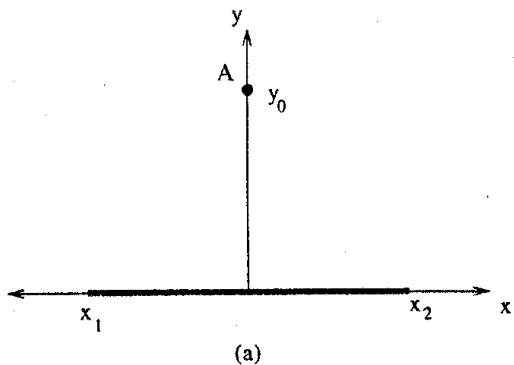

(a)

Fig. 2. (a) A finite line charge and a point A in a selected coordinate system.

(a)

(b)

(c)

Fig. 3. Newtonian potential within (a) a rectangle; (b) an "L"-shaped object; and (c) the object used in Fig. 19 of [20]. The brighter a point, the lower is the potential. The brightness is made to vary logarithmically with potential value.

4.1.2 Newtonian Force Due to Line Segments

As outlined in Section 3, once positioned on the MAT skeleton, we use the force experienced at that point to traverse the rest of the skeleton. For this purpose, we now obtain an expression for the Newtonian force at a point due to a uniformly charged line segment.

With reference to Fig. 2, the repulsive force on point A due to a point $(x, 0)$ on the x-axis can be calculated as

$$-\nabla\left(\frac{1}{r}\right) = \frac{1}{r^2}\hat{\mathbf{r}} = \frac{1}{x^2 + y_0^2}\left(\cos\theta\,\hat{\mathbf{x}} + \sin\theta\,\hat{\mathbf{y}}\right), \quad (4)$$
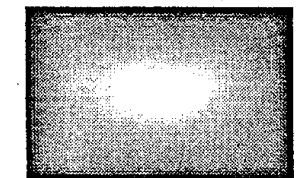
where θ is the angle of the position vector with respect to the $+x$ direction. By the superposition principle, the net force on A due to the entire line segment has the following two components:

$$F_x = \int_{x_1}^{x_2} \frac{\cos\theta\,dx}{r^2(x)} = \int_{x_1}^{x_2} \frac{-x\,dx}{\left(x^2 + y_0^2\right)^{3/2}} = \frac{1}{\sqrt{x^2 + y_0^2}}\Big|_{x_1}^{x_2} \quad (5)$$
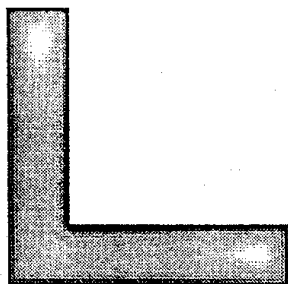
and

$$F_y = \int_{x_1}^{x_2} \frac{\sin\theta\,dx}{r^2(x)} = \int_{x_1}^{x_2} \frac{y_0\,dx}{\left(x^2 + y_0^2\right)^{3/2}} = \frac{1}{y_0\sqrt{x^2 + y_0^2}}\Big|_{x_1}^{x_2}. \quad (6)$$
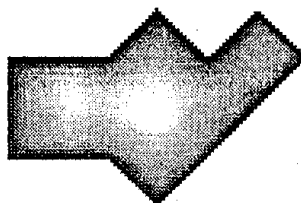
Fig. 4 shows force fields for the regions shown in Fig. 3. The force vector at a point is indicated by drawing an arrow. The arrows, or streamlines, merge along "valleys" (1D potential minima) and "converge" at points that are 2D potential minima. Clearly, the potential valleys are close to the corresponding MAT skeletons.
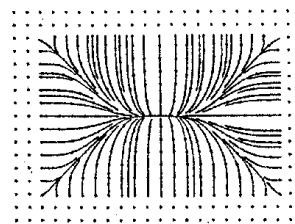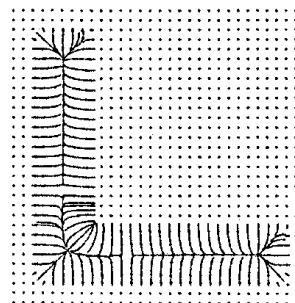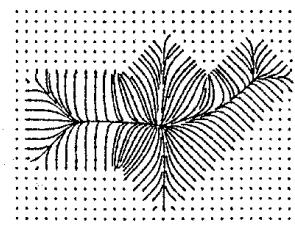

(a)

(b)

(c)

Fig. 4. Streamline representations of Newtonian force fields within regions shown in Fig. 3.

4.1.3 A MAT Algorithm

The MAT skeleton, in general, consists of potential valleys and isolated 2D potential minima. A region yields a connected component of the skeleton consisting of a single 2D minimum or a graph of potential valleys having vertices at 2D potential minima. The basic computation of the MAT skeleton, starting with an arbitrarily given point of the region called the seed point, is described in the following algorithm (see Fig. 5):
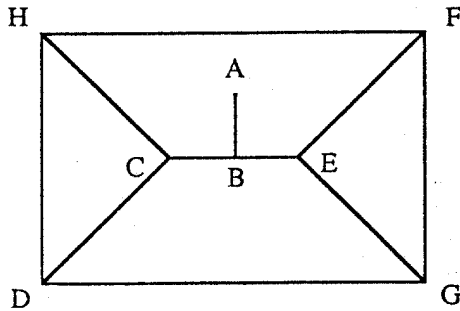

Fig. 5. The basic MAT algorithm. Starting from point *A*, following the direction of Newtonian force leads to contact with MAT at point *B*. Then, the direction towards *E* is randomly chosen (instead of towards *C*) and the valley *BE* is followed to *E*. Then *E* is used as the starting point to begin a recursive traversal of the MAT skeleton along the direction *EF*, *EC*, and *EG*.

Fig. 6. Skeletons obtained using the Newtonian potential for regions shown in Fig. 3. (a), (b), and (c) are obtained for Figs. 3a, 3b, and 3c, respectively. (d) MAT of Fig. 3b, from [21], (e) MAT of Fig. 3c, from [20].

Algorithm MAT-Newtonian-Polygon

Step 1: Reach the skeleton starting from the seed point by following the direction of the force.
Step 2: Follow the skeleton from the point of initial contact until a zero force is obtained.

Step 3: Traverse the skeleton by recursively following along each branch (out of a vertex), or by following both directions along the skeleton (out of a nonvertex) until both ends of the branch containing that point are reached.

For polygonal regions, all convex corners are end points of the medial axis. Therefore, if they are chosen as seed points, Step 1 can be avoided. Fig. 6 shows the skeletons obtained from Step 2 alone using such seed points. Similarity between these potential skeletons and the MAT can be observed by comparing Figs. 6a-6c with Fig. 1, Fig. 8c in [21] (reproduced here as Fig. 6d), and Fig. 19 in [20] (reproduced here as Fig. 6e), respectively. A skeleton, thus, obtained may not be connected, as shown in Fig. 6b.
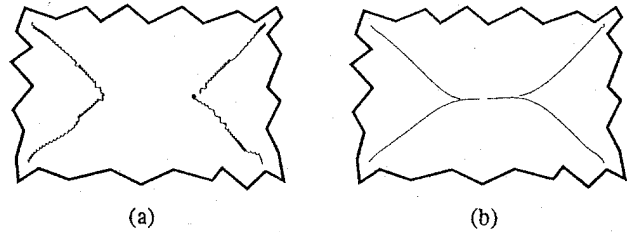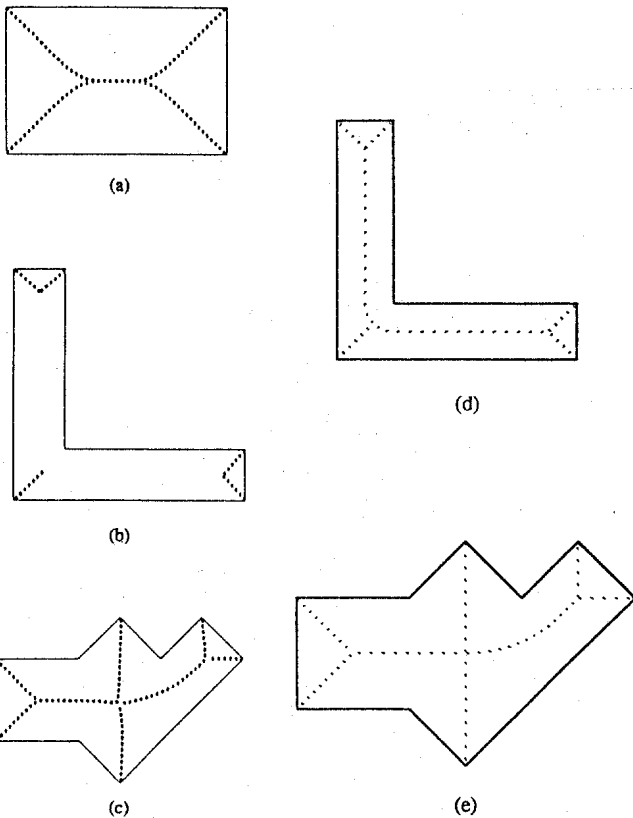

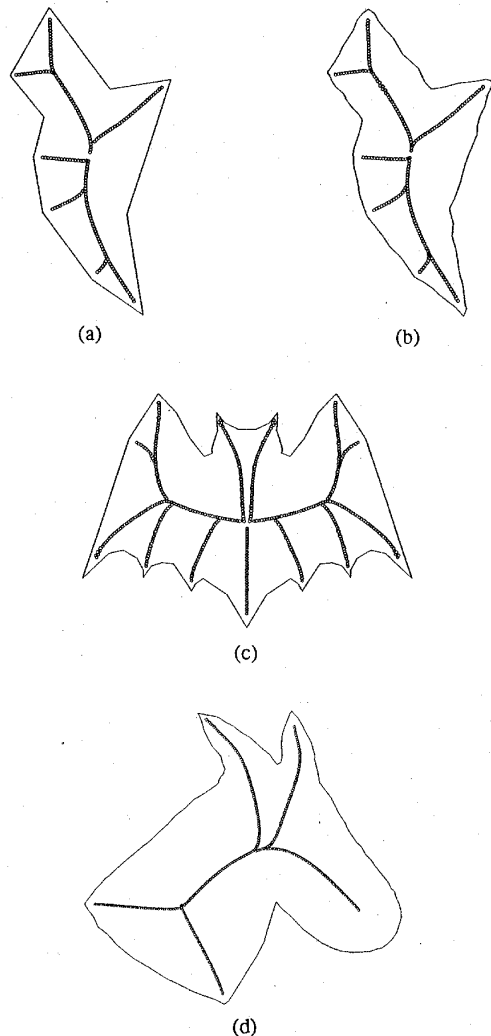Fig. 7. Force following results for obtaining (a) medical axis and (b) potential skeleton.

Fig. 8. Potential skeletons obtained for different polygonal regions. The polygonal approximation in (a) has only about 1/8 of boundary elements of that in (b).

For noisy boundary, a similar force following method is not suitable for obtaining the medial axis since a zigzag pattern like that shown in Fig. 7a will be obtained. (In this case, the gradient direction the distance function is followed.) The Newtonian skeleton is less sensitive to the fluctuations in the region boundary as can be seen from Fig. 7b. Since the Newtonian skeleton is spatially smooth, we will only show discrete samples of the skeleton in the rest of the paper.

For arbitrary shaped regions, coarse-to-fine polygonal approximations can be obtained. If the approximation error is decreased slowly, the skeletons corresponding to successive polygons will be similar. Therefore, the skeleton corresponding to an approximation can be used as initial estimate to obtain the next finer estimate. Fig. 8 shows potential skeletons obtained for different polygonal regions. The polygonal approximation in Fig. 8a has only about 1/8 of boundary elements of that in Fig. 8b, while Figs. 8b-8d have similar resolutions in the representation of their boundaries.

4.1.4 Problems with the Above Algorithm

The potential at a given point inside a region is by definition the summation of the potentials due to all boundary points everywhere; it does not depend only on the nearest border points. This leads to erroneous shifts in the potential valleys with respect to the locations of the medial axes (see Fig. 9). To avoid these problems, we use a different potential field which is discussed next [22].
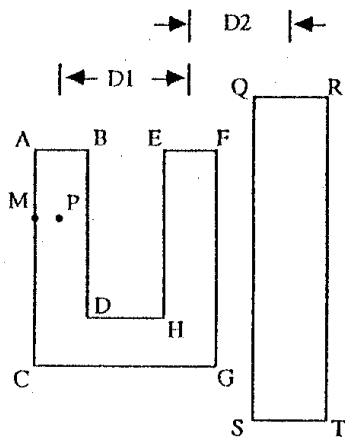

Fig. 9. The potential value at P receives a larger contribution from MC than from AM. Further, the Newtonian potential at point P depends not only on segments immediately surrounding it, i.e., on segments AB, AC, BD, CG, but also on segments EF, FG, EH, etc., as well as segments QR, RT, ST, and QS. As a result, the potential valley in the vicinity of P is shifted to the left.

4.2 A Generalized Potential Field

We now describe a generalized potential function whose purpose is to suppress the influence of the extraneous borders, as discussed above. We achieve this by observing that if the potential is made to decay faster with distance than the Newtonian potential, then the undesirable effects mentioned in Section 4.1.4 will become proportionately less severe. We achieve faster decay by using the nth order potential given by $1/r^n$ instead of the first order. For example, for point A in Fig. 2, such a generalized potential is given by

$$\int_{x_1}^{x_2} \frac{dx}{r^n}. \tag{7}$$

The two components of the corresponding repulsive force, called the nth order force, or n-force, can then be shown to be given by

$$\left(F_x, F_y\right) = \left(\int_{x_1}^{x_2} \frac{-x\,dx}{\left(x^2 + y_0^2\right)^p}, \int_{x_1}^{x_2} \frac{y_0\,dx}{\left(x^2 + y_0^2\right)^p}\right), \tag{8}$$

with $p = (n + 2)/2$. The integrals can be evaluated analytically with

$$\int \frac{x^m dx}{\left(x^2 + c\right)^p} = \frac{x^{m+1}}{2c(p-1)\left(x^2 + c\right)^{p-1}} - \frac{m - 2(p-1) + 1}{2c(p-1)} \int \frac{x^m dx}{\left(x^2 + c\right)^{p-1}}, \quad (p > 1, c > 0) \tag{9}$$

where $m = 1$ is used to evaluate the x-component and $m = 0$ to evaluate the y-component of the repulsive force. The larger the value of n used in defining the generalized potential, the lower the extraneous effects, because the direction of the force at a point not positioned on the medial axis can be made arbitrarily close to that pointing away from the closest border point. This leads us to the following result:

Suppose we are given a 2D polygonal region and its medial axis which partitions the region into cells such that points within each region are closest to exactly one polygon edge. Then, the direction of the n-force will converge to that of the gradient of the shortest distance function at any point inside a cell if n increases indefinitely.

Therefore, if the potential valleys are traversed in the same manner as in the Newtonian potential case, the resulting n-skeleton should converge to the true skeleton. Fig. 10 shows the effect of increasing the order of the potential function on the corresponding force field for the rectangular region discussed earlier. This suggests that to find MAT we require n-skeletons for large values of n. We now present an algorithm for computing n-skeleton from the $(n-1)$-skeleton, $n > 1$. Let P denote the point on the $(n-1)$-skeleton whose successor Q on the n-skeleton is to be found, and θ_0 be the direction perpendicular to the $(n-1)$-force at P, as shown in Fig. 11. The following algorithm finds Q with accuracy $s_{\min}$ by conducting a binary search for it.
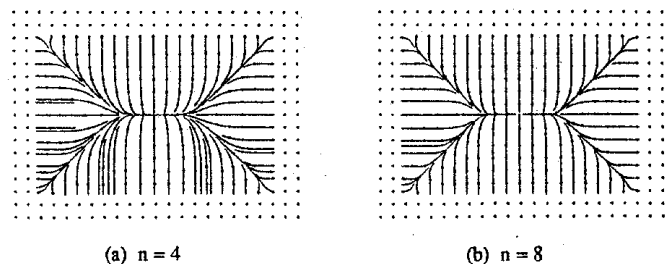

(a) n = 4   (b) n = 8

Fig. 10. Streamline representations of force fields due to generalized potential of different orders within the region shown in Fig. 3a.

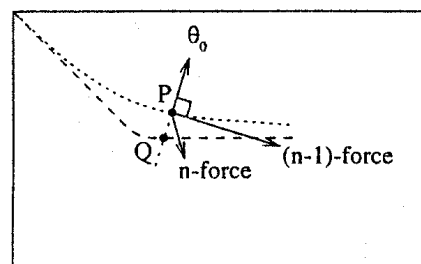Fig. 11. A point P on the $(n-1)$-skeleton (dotted line). The successor of P, Q, on the n-skeleton (dashed line) can be found along the projection of the n-force at P along θ_0 which is perpendicular to the $(n-1)$-force at P.

Algorithm Successor

Step 0: Find the direction of θ_0. Initialize (spatial) step size $s = S$ where S is a given constant.

Step 1: Compute the n-force at P and find its projection along θ_0. If the projection along θ_0 is 0, i.e., the n-force is perpendicular to θ_0, let $Q = P$ and go to Step 5.

Step 2: Locate the point Q, which is a distance s away from P along the projected force direction.

Step 3: If $s \geq s_{min}$ and the above projected force has not reversed its direction so far, then let $P \leftarrow Q$, and go to Step 1.

Step 4: If $s \geq s_{min}$, then let $s \leftarrow s/2$, $P \leftarrow Q$, and go to Step 1.

Step 5: Q is the desired successor of P on the n-skeleton.

By finding successors for all points on the $(n-1)$-skeleton, we can find the n-skeleton from the $(n-1)$-skeleton. (As a matter of fact, an n'-skeleton, $1 \leq n' < n$, can also be used in place of the $(n-1)$-skeleton in the above algorithm, as will be considered later.) In the next section, we develop an nth order potential field-based MAT algorithm.

4.3 A Generalized-Potential Field Based MAT Algorithm

The accuracy of the MAT skeleton obtained using a given n value can be expressed in terms of the maximum deviation between the n-skeleton and the true skeleton. The maximum deviation must be less than some threshold distance e_{min} to be acceptable. To reduce the displacement between the potential valleys and the medial axis, we need to increase the value of n. However, the complexity of the computation of the n-force increases with n. Also, the numerical error due to finite resolution accumulates for larger values of n. Therefore, it is desirable to use as small a value of n as possible while still ensuring the desired accuracy of the MAT. We will refer to the n-skeleton obtained for the smallest acceptable n value as ∞-skeleton. We have already seen that as $n \rightarrow \infty$, ∞-axis $\equiv$ medial axis.

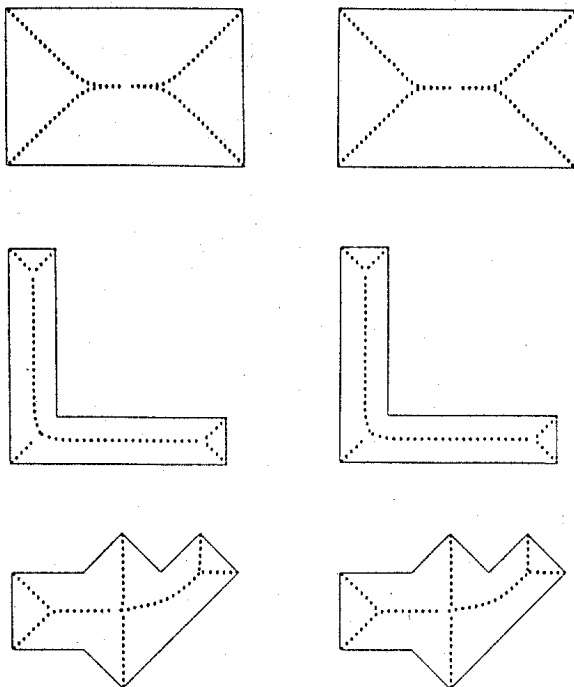

Fig. 12. *N*-skeletons obtained for the regions shown in Fig. 3 for *N* = 4. (left) and *N* = 8 (right).

A straightforward algorithm to obtain ∞-skeleton is to start with the Newtonian skeleton, and generate n-skeletons for increasing value of n (e.g., the skeletons shown in Fig. 12)

until the maximum difference between the $(n-1)$-skeleton and the n-skeleton is less than e_{min}. An immediate, simple solution to the above problem is to not consider further generation of successors of a point for an n value beyond which the change in its location is less than e_{min}. (Let N_P denote such an n for a point P on the Newtonian skeleton.) This simple solution can be modified further so that it is computationally more efficient. Note that the direction of the force at any nonskeleton point must ultimately converge to the direction pointing away from the nearest boundary point (see the force fields for the rectangular object in Fig. 10). Thus, if we increase the value of n successively, and each time compute the change in direction of the n-force at P, then the smallest value of n, denoted as N_P', for which the above change will be smaller than a fixed value, θ_{min}, for all $n > N_P'$ could serve as an estimate of N_P, as described in the following algorithm. (The subscript of N_P is omitted for brevity.)

Algorithm MAT-Generalized-Polygonal

Step 0: (Start with $N = 2$ as the estimate of the lowest acceptable value of n for point P.)
Initialize $N = 2$.

Step 1: (Increase N if doing so changes θ_N significantly.)
If $|\theta_N - \theta_{N-1}| > \theta_{min}$, then let $N = N + 1$ and go to Step 1, where θ_N is the direction of N-force at P.

Step 2: (Ensure that two successive N values yield insignificant changes in N.)
If $|\theta_{N+1} - \theta_N| > \theta_{min}$, then let $N = N + 1$ and go to Step 1.

Step 3: (The minimal required order of the generalized potential has been estimated for P.)
Find the successor of P, Q, on N-skeleton directly by using N-force and Steps 1-5 of the algorithm *Successor*. Q is the desired medial axis point corresponding to P.

Since the amount of direction change ($\Delta\theta$) may not be monotonic with increasing n, an additional check is carried out in Step 2 to refine the estimate, so that Step 1 will not be confused by a wide, shallow valley of $\Delta\theta$ before it breaks up again. Fig. 13 shows $p = (N_P + 2)/2$ at different skeleton locations for the rectangular region shown in Fig. 3a with
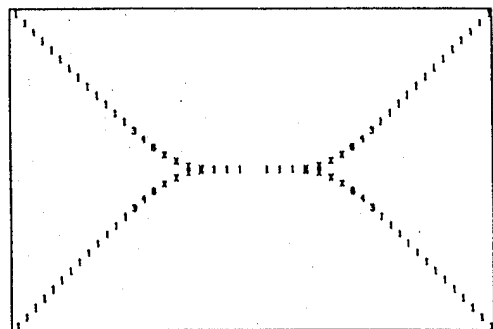
$$\theta_{min} = \cos^{-1}(0.999) = 2.56°.$$

Fig. 13. The smallest values of $p = (N + 2)/2$ at different skeleton locations for the rectangular region shown in Fig. 3a. The smallest value is computed to ensure that the change in the direction of the pth and $(p-1)$th force fields, and the $(p-1)$th and $(p-2)$th force fields, is less than $\cos^{-1}(0.999) = 2.56°$.

An "*x*" is displayed if $p > 9$ is needed. Larger ps are needed for locations where the ∞-skeleton lies farther away from the potential skeleton, i.e., near the junction points in this case.

5 IMPLEMENTATION AND EXPERIMENTAL RESULTS

A simplified form of the algorithm *MAT-Newtonian-Polygonal* of Section 4.1.3 was implemented. Step 2 (force following) of this algorithm is implemented using convex polygon corners as seeds. Translation of a fixed step size is performed along the *n*-force ($n = 1$), which is evaluated in closed form. The translation stops when the force reverses its direction since the exact location at which the force is 0 may be overshot due to the nonzero step size, which is chosen to be about 1% of the dimensions of the corresponding regions. Fig. 6 shows the MAT skeletons obtained for three different polygons. The skeletons are shown with a sampling distance twice that of the step size. The computation times for Figs. 8b, 8c, and 8d are 0.37, 0.33, and 0.71 second, respectively, on a Sun Sparc 10/51 Workstation.

For the implementation of algorithm *Successor* of Section 4.2, the direction θ_0 in which the binary search is carried out is chosen to be perpendicular to the Newtonian skeleton direction. The latter is estimated at a skeleton point by averaging the directions of the Newtonian forces at that point and at the neighboring skeleton points which have a higher potential values. The *n*-force is considered as perpendicular to θ_0 in Step 1 of algorithm *Successor* if the angle between the force direction and θ_0 is within

$$90° \pm \sin^{-1}(0.001) = 90° \pm 0.057°.$$

For results obtained in Fig. 12, the initial step size S in *Successor* is chosen as 1% of the region dimension, and the minimal search step $s_{\min}$ is chosen to be 1/8 of the initial step size.

6 COMPARISONS WITH OTHER SKELETONIZATION METHODS

6.1 The Geometric Approach in [16]

A hierarchical algorithm based on the definition of the medial axis is presented in [16] for deriving the axis for a simple polygonal region. Although the complexity of the algorithm is O(*n* log *n*), where *n* is the number of convex vertices, the implementation of the algorithm is complicated. Moreover, for a noisy region border which is often found in a digital image, the complete medial axis may have a lot of branches of little significance. For example, *n* is equal to 40 for the region shown in Fig. 8b. In order to obtain a portion of the axis similar to that shown in Fig. 8b, the whole axis has to be derived first before further pruning of the axis is performed. Finally, since the medial axis is formed by connecting linear or parabolic curves, the axis will not be as spatially smooth as those shown in Fig. 8. The smoothness property is desirable in some motion planning applications of the medial axis, e.g., in [23].

6.2 A Thinning Algorithm

In order to identify the skeleton points in a digital image, thinning algorithms which iteratively delete the nonskeleton border points of a 2D region are often used. Whether a point should be deleted or not can be determined by simply examining the local neighborhood of that point [24]. Fig. 14 shows the thinning result for the 2D region shown in Fig. 8a, in an equivalent 240 × 360 binary image format. The computation time for deriving the skeleton is about 2.2 seconds on a Sun Sparc 10/51 Workstation. Notice that several branches of the skeleton shown in Fig. 8a are missing in Fig. 14. Moreover, the connectivity of the skeleton is not guaranteed with this simple implementation. Finally, certain portions of the resulting skeleton are not thinned to unit width.
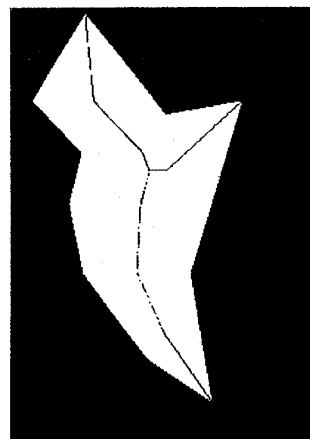

Fig. 14. The thinning result obtained according to [24] for the 2D region shown in Fig. 8a, in an equivalent 240 × 360 binary image format.

7 SUMMARY

In this paper, we have considered the problem of efficient computation of the MAT representation of objects from given border data. The central theme of the approach we have presented is the use of a potential field to represent the available object shape information. The potential value captures the information about the distances of an interior point to different border segments into a single scalar potential. In addition, the closed-form expression of the gradient of the potential is derived and used to improve the accuracy and efficiency in locating the potential valley by force following. The potential valley is continuous, and its location is spatially smooth and insensitive to noises in the object border. By using the *n*th order potential given by $1/r^n$, it is shown that the potential valley converges to the medial axis as *n* approaches infinity. The algorithms presented can generate part of the axis without the need to derive the complete axis first. The algorithms can also be used as thinning algorithms.

REFERENCES

[1] H. Blum, "A Transformation for Extracting New Descriptors of Shape," *Models for the Perception of Speech and Visual Form*, W. Wathen-Dunn, ed., Cambridge, Mass.: MIT Press, 1967.

[2] A. Rosenfeld and J.L. Pfaltz, "Distance Functions on Digital Pictures," *Pattern Recognition*, vol. 1, pp. 33-61, 1968.

[3] G. Borgefors, "Distance Transformations in Arbitrary Dimensions," *Computer Vision, Graphics, and Image Processing*, vol. 27, pp. 321-345, 1984.

[4] P.P. Das and P.P. Chakrabarti, "Distance Function in Digital Geometry," *Information Sciences*, vol. 42, pp. 113-136, 1987.

[5] G. Borgefors, "Distance Transformations on Hexagonal Grids," *Pattern Recognition Letters*, vol. 9, pp. 97-105, 1989.

[6] A. Rosenfeld and A.C. Kak, *Digital Picture Processing*. New York: Academic Press, 1976.

[7] P.E. Danielson, "Euclidean Distance Mapping," *Computer Vision, Graphics, and Image Processing*, vol. 14, pp. 227-248, 1980.

[8] N. Ahuja, L.S. Davis, D.L. Milgram, and A. Rosenfeld, "Piecewise Approximation of Pictures Using Maximal Neighborhoods," *IEEE Trans. Computers*, vol. 27, pp. 375-379, 1978.

[9] F. Meyer, "The Binary Skeleton in Three Steps," *Computer Architecture for Pattern Analysis and Image Database Management*. New York: IEEE CS Press, 1985.

[10] F. Meyer, "Skeletons and Perceptual Graphs," *Signal Processing*, pp. 335-363, 1989.
[11] A. Montanvert, "Medial Line, Graph Representation, and Shape Description," *Proc. Eighth Int'l Conf. Pattern Recognition*, Paris, France, pp. 430-432, 1986.
[12] L. Dorst, "Pseudo-Euclidean Skeleton," *Proc. Eighth Int'l Conf. Pattern Recognition*, Paris, France, pp. 286-288, 1986.
[13] Y. Xia, "Skeletonization via the Realization of the Fire Front's Propagation and Extinction in Digital Binary Shapes," *IEEE Trans. Pattern Analysis and Machine Intelligence*, vol. 11, pp. 1,076-1,086, 1989.
[14] U. Montanari, "Continuous Skeletons from Digitized Image," *J. ACM*, vol. 14, pp. 534-549, 1969.
[15] D.G. Kirkpatrick, "Efficient Computation of Continuous Skeletons," *Proc. 20th Ann. IEEE Symp. Foundations of Computer Science*, pp. 18-27, Oct. 1979.
[16] D.T. Lee, "Medial Axis Transformation of a Planar Shape," *IEEE Trans. Pattern Analysis and Machine Intelligence*, vol. 4, pp. 363-369, 1982.
[17] C.K. Yap, "An O(*n* log *n*) Algorithm for the Voronoi Diagram of a Set of Simple Curve Segments," Robotics Lab. Report No. 43, Courant Inst., New York Univ., New York, 1985.
[18] J.-H. Chuang, "Skeletonization of Three-Dimensional Regions Using Generalized Potential Field," *Proc. Int'l Conf. Control and Robotics*, Vancouver, Canada, Aug. 1992.
[19] J.-H. Chuang, "Skeletonization Using the Newtonian Potential," *Proc. Int'l Computer Symp.*, Hsinchu, Taiwan, R.O.C., pp. 639-644, 1990.
[20] H. Blum and R.N. Nagel, "Shape Description Using Weighted Symmetric Axis Features," *Pattern Recognition*, vol. 10, pp. 167-180, 1978.
[21] K.S. Fu, R.C. Gonzalez, and C.S.G. Lee, *Robotics*. New York: McGraw-Hill, 1987.
[22] W. Chew, *Personal Communication*, 1990.
[23] O. Takahashi and R.J. Schilling, "Motion Planning in a Plane Using Generalized Voronoi Diagrams," *IEEE Trans. Robotics Automation*, vol. 5, no. 2, pp. 143-150, 1989.
[24] T.Y. Zhang and C.Y. Suen, "A Fast Parallel Algorithm for Thinning Digital Patterns," *Comm. ACM*, vol. 27, pp. 236-239, 1984.